Original paper: https://doi.org/10.1016/j.engstruct.2018.11.008
This work is licensed under a Creative Commons Attribution-NonCommercial-NoDerivatives 4.0 International License.

Shear Strengthening of Concrete Members with Unbonded Transverse Reinforcement

Mathieu Fiset[a], Josée Bastien[b], Denis Mitchell[c]

[a] Département de génie civil et de génie des eaux, Université Laval, 1065, av. de la Médecine, Québec (Québec), G1V 0A6, Canada, mathieu.fiset.1@ulaval.ca (Corresponding author)

[b] Département de génie civil et de génie des eaux, Université Laval, 1065, av. de la Médecine, Québec (Québec), G1V 0A6, Canada, josee.bastien@gci.ulaval.ca

[c] Department of Civil Engineering and Applied Mechanics, McGill University, 817 Sherbrooke Street West, Montreal (Quebec) H3A 0C3, Canada, denis.mitchell@mcgill.ca

Declarations of interest: none

ABSTRACT

This paper examines the behaviour of thick concrete members strengthened in shear with unbonded transverse reinforcement. The retrofitting technique consists of placing unbonded vertical bars with steel end plates or torque controlled expansion end anchorages in pre-drilled holes of existing thick members. To study the behaviour of these members, loading tests as well as numerical analyses were carried out. Shear capacities were compared to the predictions using the shear design approach in the Canadian Highway Bridge Design Code. The design equations which are intended for traditional stirrups reinforcement overestimates the shear capacities of the members strengthened with unbonded transverse reinforcement. However, numerical analyses provided very accurate predictions of the shear capacities. A finite element parametric study examines the effects of the shear span-to-depth ratio, vertical prestressing, shear reinforcement ratio and the stiffness of the vertical reinforcement. The stiffness of the shear strengthening system and the effects of prestressing significantly affect the shear capacity. The shear capacities were predicted well when a minimum amount of vertical prestressing was provided.

Key words: Reinforced Concrete, Shear Strengthening, Shear Behaviour, Shear Strength, Unbonded bars, Finite Element Modelling

1. INTRODUCTION

Numerous concrete bridges have been subjected to concrete degradation, steel corrosion as well as increased loading and frequency of traffic. This may result in insufficient flexural and shear capacities. The one-way shear failure of the “La Concorde” overpass in Laval (Canada) in 2006 showed that many thick concrete slab bridges without shear reinforcement may require shear strengthening [1, 2]. This event is one of many examples illustrating the fact that shear failure of concrete members without shear reinforcement is very brittle. The critical diagonal crack propagates rapidly accompanied by a sudden drop in shear capacity, often without any warning of the impending failure. To prevent such a brittle failure mode, concrete thick slabs should contain a minimum amount of shear reinforcement [1]. Members with an appropriate minimum amount of shear reinforcement are capable of redistributing the stresses and controlling shear cracking.

Adhikary and Mutsuyoshi [3] have tested several shear strengthening techniques in beams. They found that the most effective method to increase the member shear capacity consisted of clamping transverse reinforcing bars on the existing concrete member and to anchor the bars extremities using mechanical anchorages. Unlike conventional transverse reinforcement (stirrups installed before concrete casting), the added bars are typically unbonded to the concrete. Although this clamped shear strengthening technique has been commonly used by engineers, only a limited number of studies are devoted to shear failure investigations for members with shear span-to-depth ratio (a/d) over 2.5. Many authors have studied flexural failures of shear strengthened beams with vertical unbonded bars, but very few studied the influence on the shear failure behaviour. The effects of unbonded transverse reinforcement on the shear strength of slender beams were studied experimentally by Suntharavadivel [4], Elstner and Hognestad [5] and Lechner and Feix [6], while Ferreira, Bairán et al. [7] performed finite element analyses. These authors have observed that before shear cracking, unbonded transverse reinforcement shows almost no increase in strain. However, at the shear cracking load, strains in the unbonded bars increased until beam failure occurred. After diagonal cracking, the shear is transferred to the shear reinforcement until the critical diagonal crack becomes so large that shear failure occurs. This behaviour was also observed for deep beams and slabs [3, 4, 8-10].

By keeping the total transverse reinforcement ratio (ρ_v) constant and progressively replacing stirrups by unbonded bars, Altin, Tankut et al. [11] showed that the same failure mode and similar load capacities can be achieved. However, they observed that replacing embedded stirrups by unbonded bars reduces the member deformation capacity. Shear strengthened beams with only unbonded reinforcement also showed only a small number of diagonal cracks compared to beams with internal stirrups. Elstner and Hognestad [5], Khaloo [12], Shamsai, Sezen et al. [13] have also shown that prestressing the unbonded vertical bars enables a further increase of the shear capacity so that the failure mode may shift from a brittle shear to a ductile flexural failure.

1.1. Research significance

This paper focuses on the behaviour of thick concrete members, representing thick slabs, that has been strengthened using unbonded drilled-in transverse reinforcement. This retrofitting consisted of inserting bars in pre-drilled holes into an existing member and anchoring the bars with steel end plates or torque-controlled expansion anchorages. These two techniques can be used for the shear retrofit of thick concrete slabs, particularly those without any stirrups. A complementary finite element (FE) investigation was performed to better understand the shear behaviour of such members. In addition, a parametric study was carried out to examine the effects of the shear span-to-depth ratio, vertical prestressing, the shear reinforcement ratio and the stiffness of the shear strengthening system on the shear behaviour.

2. EXPERIMENTAL PROGRAM

2.1. Strengthening Techniques

Experimental tests were carried out on beams representing slices of thick concrete slabs. The retrofitting consisted of drilling vertical holes into the existing concrete structure and inserting a reinforcing bar in each hole. For practical considerations, drilling of holes and bars installation are typically performed from the top of the member. Two shear strengthening systems illustrated in Fig. 1 were used. Fig. 1a presents mechanically anchored treaded bars (hole diameter d_h = 24.0 mm, bar diameter d_b = 15.9 mm with a net bar area A_b = 146 mm²) used to strengthen beam specimens type T in Fig. 2. The lower bar extremity is anchored with torque controlled expansion anchorages and an anchor plate is installed to anchor the top extremity at the beam top surface. When torqued, the expansion of the bottom anchor exerts lateral pressure on the internal surface of the hole, which produces frictional forces to provide anchorage. Another shear strengthening system (Fig. 1b) was used for specimens type P (see Fig. 2) which consists of inserting high-strength #9 reinforcing bars (d_h = 40.0 mm, d_b = 28.7 mm, A_b = 645 mm²) with threaded ends into drilled holes and anchored with nuts and plates at the top and bottom of the concrete beam surfaces. The main advantage of these two strengthening techniques is that they can be used in wide beams or structural thick slabs to resist shear. The strengthening technique used in type T members can be used in a positive moment region to avoid cutting longitudinal tension reinforcement located in the bottom of a member during the installation procedure. Otherwise, the strengthening technique used in type P members can be used in a negative moment region or when drilling can easily be performed avoiding cutting through the longitudinal tension reinforcement.

For comparison purposes, two additional sets of beams were tested (Fig. 2). Specimens type S contained conventional stirrups (d_b = 15.9 mm and A_b = 200 mm²) installed before the concrete was cast while specimens type U represent control specimens that did not contain any shear reinforcement and was not retrofitted.

2.2. Details of Test Specimens

The specimen dimensions, material properties and strengthening details are summarized in Table 1 and Fig. 2. All of the test specimens span 4 m, have a total height, h, of 750 mm and a width, b_w, of 610 mm. A normal-strength concrete with a maximum aggregate size, a_g, of 20 mm was used. The concrete compressive strength, f'_c and Young's modulus, E_c, were measured on cylinders according to ASTM-C39, ASTM-C469, respectively and the average properties are summarized in Table 1.

Specimen type U contains one layer of longitudinal reinforcing bars (nominal bar diameter, d_b, of 25.2 mm) located at a effective depth, d, of 699 mm, having a total area, A_s, of 5000 mm² and a yield strength, f_y, of 468 MPa. Specimen types S, T and P contain a total area of longitudinal reinforcement A_s = 7000 mm² at d = 694 mm and having f_y = 508 MPa and d_b = 29.9 mm.

While specimen type U did not contain any shear reinforcement, specimen types S, T and P were designed to have more than the minimum amount of shear reinforcement $\rho_{v,min}$ required by CSA-S6 [14] (see Eq. (1)). The stirrups used in the specimens type S have a total area A_v of 400 mm² and were installed at a spacing s of 380 mm (shear reinforcement ratio $\rho_v = A_v / (b_w s)$ = 0.17%). Specimens type T was shear strengthened with vertical bars having A_v = 292 mm², s = 380 mm, ρ_v = 0.13% and anchored with torqued controlled expansion anchorage. The tensile capacity F_u of the torque controlled anchorages is 90.8 kN according to the compressive strength of the concrete mix used [15]. Specimens type P have one set of bars in the middle of the shear span so that the total area A_v is 1290 mm². Young modulus, E_s = 200 000 MPa, hardening strain, ε_{sh} = 2.3% and strain at failure, ε_u = 18% were measured on stirrups and were consider similar for all steel used. The other mechanical properties of shear reinforcing bars are summarized in Table 1, where f_u is the tensile strength.

$$\rho_{v,min} = 0.06\frac{\sqrt{f_c'}}{f_y} \quad \text{(MPa units)} \tag{1}$$

2.3. Test Setup and Instrumentation

The test setup is shown in Fig. 2. The loading was applied in several load steps at a constant midspan deflection rate of 0.17 mm/min. The shear span, a, was 2000 mm so that the shear span-to-depth ratio a/d was about 2.9. At each load stage, the midspan deflection was kept constant while measurements were taken. After the occurrence of a shear failure in one half of the beam, the specimen was unloaded and steel shear clamping devices were added to the failed half span in order to reload the beam until failure of the other half span. The midspan deflection was monitored using a linear variable differential transformer (LVDT) and the applied load was measured using a load cell. Strain gauges were installed to measure the transverse reinforcing bar strains (Fig. 2). LVDTs in a form of rosettes were installed on the side faces of the beams at the middle of the shear spans.

2.4. Experimental Results

Table 2 and Fig. 3 to Fig. 5 summarize the experimental results. In Fig. 3 showing the cracking of the specimens at failure, the diagonal crack leading to the shear failure is represented with a bold line while the other experimental cracks are identified with thinner lines. As observed by Altin, Tankut et al. [11], specimens with stirrups (S1 and S2) in Fig. 3 exhibited a larger number of diagonal cracks than the specimens with unbonded bars (types T and P). For comparison, the specimens without shear reinforcement (type U) and shear strengthened specimens type T exhibited only one large critical shear crack while specimens P1 and P2 experienced two diagonal cracks; the larger one leading to failure. For the specimens with stirrups, S1 and S2, the strain in the shear reinforcement increased when the first diagonal crack at cracking shears, V_{cr} , of 495 kN and 484 kN, respectively. Specimens S1 and S2, with stirrups, failed at a shear of 726 kN and 809 kN, respectively. Fig. 6 shows some selected strain measurements for specimen S2 indicating that yielding of the stirrups occurred (refer to Fig. 2 for transverse reinforcement numbering and strain gauge locations). Fig. 6 also compares the difference in strains measured in the top and bottom portions of the stirrups.

For specimens without shear reinforcement (type U), shear failure occurred shortly after the sudden propagation of a large diagonal crack. This sudden crack propagation was also observed for the specimens with unbonded shear reinforcement but did not lead to immediate failure. The shear cracking propagation is responsible for the observed peaks of the shear versus deflection curve, at about 490 kN, as shown in Fig. 4. Each of these intermediate peaks was followed by the sudden propagation of a large diagonal crack and reductions in shear of about 85 kN and 60 kN on average for specimens T and P, respectively. The sudden propagation of a large diagonal crack and the associated decrease in load was not observed for beams with stirrups (S1 and S2). The influence of shear failure on one side followed by unloading, shear strengthening and reloading is apparent from the load versus deflection responses shown in Fig. 6.

Before shear cracking, the unbonded shear reinforcing bars in specimens type P experienced low strains (Fig. 6) and opening of a diagonal crack is required to activate the unbonded bars. For specimens P1 and P2, the strains increased from 150 to 632 microstrains (f_s= 30 to 127 MPa) and from 175 to 471 microstrains (f_s= 35 to 94 MPa) after the crack propagation respectively. After their activation, the transverse bars carry some additional shear.

After initial shear cracking, no new diagonal cracks propagated in specimens T1 and T2 up to the shear failure while two diagonal cracks formed at shears of 696 kN and 671 kN in specimens P1 and P2, respectively. Failure of specimen P1 occurred shortly after initiation of the second diagonal crack (V_{exp}= 717 kN) and at a higher shear of 969 kN for P2. The failure of both specimens P1 and P2 occurred after crushing of the concrete and significant slip, δ, of the critical diagonal crack. At failure, the average strains of the transverse bars were 1585 and 2215 microstrains (f_s = 317 and 443 MPa) for P1 and P2, respectively. These measured strains indicated stresses below the yield stress of the reinforcing bars (f_y = 517 MPa).

The additional shear capacity offered by shear strengthening can be determined by comparing the maximum experimental capacity, V_{exp}, to the capacity at diagonal cracking, V_{cr}. In average, the addition of unbonded shear reinforcement led to a shear capacity increase of about 20% and 72% (V_{exp} / V_{cr}) for specimens T and P, respectively. This ratio is an indicator of the efficiency of the shear strengthening techniques.

3. MODIFIED COMPRESSION FIELD THEORY

The modified compression field theory (MCFT) [16-18] enables the determination of the shear behaviour of elements with and without shear reinforcement. According to the MCFT, the shear nominal capacity, V_n, is the summation of the shear carried by the concrete V_c and by the transverse reinforcement V_s according to Eq. (3) and (4), where f_{c1} is the tensile stress in cracked concrete (Eq.(5)) limited by the aggregate interlock capacity v_{ci} in Eq. (6), d_v the effective shear depth taken as $0.9d$, f_s is the bar stress and $d_v \cot\theta / s$ being the amount of shear reinforcement crossing the diagonal cracks.

$$V_n = V_c + V_s \tag{2}$$

$$V_c = f_{c1} \cot\theta b_w d_v \leq v_{ci} b_w d_v \tag{3}$$

$$V_s = \frac{A_v f_s d_v \cot\theta}{s} \tag{4}$$

$$f_{c1} = \frac{f_{cr}}{1+\sqrt{c\,\varepsilon_{c1}}} \tag{5}$$

$$v_{ci} = \frac{0.18\sqrt{f_c^{'}}}{0.31+24w/\left(16+a_g\right)} \quad \text{(MPa, mm units)} \tag{6}$$

The simplification of these equations led to the shear design method used in the codes in Eq. (7) to (11) [14]. The nominal concrete shear capacity is determined from the factor β in Eq. (9) (SI units), which results from the simplification of Eq. (5) with c = 500 and Eq. (6). It considers the average horizontal strain ε_x in Eq. (10), for the case of moment and shear only, and the equivalent crack spacing s_{ze}, which is taken as 300 mm for members respecting $\rho_{v,min}$ defined by Eq. (1), or as $35d_v / \left(15+a_g\right)$ otherwise. The nominal transverse reinforcement shear capacity considers no slip between concrete and shear reinforcement ($\varepsilon_c = \varepsilon_s$) and their yielding at shear failure (f_s = f_y). The angle of the compression field θ with respect to the longitudinal member axis is determined by Eq. (11) for members with shear reinforcement.

$$V_c = \beta\sqrt{f_c'}\, b_w d_v \quad \text{(MPa, mm units)} \tag{7}$$

$$V_s = \frac{A_v f_y d_v \cot(\theta)}{s} \tag{8}$$

$$\beta = \left(\frac{0.4}{1+1500\varepsilon_x}\right)\left(\frac{1300}{1000+s_{ze}}\right) \text{ (mm units)} \tag{9}$$

$$\varepsilon_x = \frac{M/d_v + V}{2E_s A_s} \tag{10}$$

$$\theta = 29 + 7000\varepsilon_x \tag{11}$$

4. FINITE ELEMENTS MODELLING

4.1. Mesh Description

The finite element (FE) program VecTor2 [19] was used to study the behaviour of the specimens and the parameters influencing their behaviour. The modelling approach is based on the MCFT [18] and Disturbed Stress Field Model (DSFM) [20]. Because of the geometry involved and loading symmetry, half of each beam was modelled (see Fig. 7 for typical mesh layout).

Fig. 8 illustrates the chosen approach to model the bars and anchorages. Two-dimensional discrete truss elements were used to simulate the transverse reinforcing bars and the longitudinal reinforcement. For conventional stirrups perfect bond was assumed between the bar and the concrete (see Fig. 8a) so that $u_s = u_c$. For the truss element representing unbonded bars, only the far extremities of the truss element are linked to the anchor elements nodes (Fig. 8b and c). To simulate the anchor plate (specimen types T and P), truss elements extremities are linked to bearing elements installed on the top of beams. The stiffness of these bearing elements is determined according to the stiffness of the anchor system. To simulate the torqued-controlled anchor behaviour (specimen type T), contact elements are used to allow slippage between the concrete and the steel bars at the bottom anchorage locations (Fig. 8c).

4.2. Material Behaviour

The adopted concrete and steel stress-strain behaviour are illustrated in Fig. 9. As shown in Fig. 9a, the tensile behaviour of plain concrete is linear up to the cracking strain, ε_{cr}, and the cracking strength f_{cr} (assumed as $0.33\sqrt{f_c'}$). It respects the tension softening proposed by Yamamoto and Vecchio [21] after cracking. The post cracking tensile behaviour of reinforced concrete considers tension stiffening according to Eq. (5), where c is the tension stiffening coefficient determined according to the reinforcement ratio [20, 22-24]. At a crack, the aggregate interlock limits the concrete tensile stress and the resulting crack slip, δ , is determined according the approach proposed by Vecchio and Lai [25]. The dowel effect is implicitly considered in the FE model by reducing the shear demand at crack, which reduces the crack slip and increases the shear capacity [19].

In compression, the modified Popovics relationship [19, 26, 27] illustrated in Fig. 9b (f_{c2} is the concrete compressive stress and ε_p is the compressive strain at peak stress f_p) was chosen and the behaviour takes into account the concrete confinement effect and the compression softening effect [28, 29]. The steel behaviour in Fig. 9c is bilinear up to the strain hardening strain, ε_{sh} , (Eq. (12)). The hardening stress-strain relationship is given by Eq. (13), where P is the strain-hardening parameter taken as 1 for steel plate elements and 4 for truss bar elements.

$$f_s = E_s\,\varepsilon_s \le f_y \quad \varepsilon_s \le \varepsilon_{sh} \tag{12}$$

$$f_s = f_u + \left(f_y - f_u\right)\left(\frac{\varepsilon_u - \varepsilon_s}{\varepsilon_u - \varepsilon_{sh}}\right)^P \quad \varepsilon_{sh} < \varepsilon_s \le \varepsilon_u \tag{13}$$

The force-slip relationship shown in Fig. 9d is used to simulate the anchor axial behaviour in specimens type T was fitted to experimental tests performed by Collins, Klingner et al. [30] and Hilti [31]. The initial anchor stiffness is taken as 14 kN/mm up to $0.35 F_u$. The anchor maximum capacity is reached at a displacement s_u of 7.5 mm on average. It decreases up to $3s_u$ with a residual capacity of $0.9F_u$.

5. COMPARISONS OF PREDICTIONS WIDTH RESULTS

5.1. The Canadian Highway Bridge Design Code (CHBDC)

It can be seen in Table 2 that the shear capacities of the specimens with stirrups and without shear reinforcement are predicted well (V_n / V_{exp} = 1.07) by the code provisions while, as expected, it greatly overestimates (V_n / V_{exp} = 1.27) the capacity of the specimens with unbonded shear reinforcement. This overestimation of shear strength is explained by the fact that the bars are unbonded and hence are not as effective in controlling diagonal cracks. The code CSA-S6 [14] considers that s_{ze} = 300 mm for members with $\rho_v \geq \rho_{v,min}$. Even if this minimum ratio is respected for specimen types T and P, they experienced a smaller number of diagonal cracks and a larger crack spacing in comparison to specimens S1 and S2. Crack width, w, and crack spacing is influenced by the bond between concrete and reinforcing bars [32-35]. Therefore, unbonded shear reinforcing bars are not as effective in controlling the crack spacing.

While the standard design method is applicable for elements with conventional bonded stirrups it is not applicable for elements with unbonded shear reinforcement. Finite element models are more appropriate to predict the behaviour of a member with unbonded shear reinforcement.

5.2. Finite Element Predictions

The finite element (FE) analysis provided very good predictions of the overall behaviour, including the shear capacity. Fig. 3 to Fig. 6 compare the predicted responses from the FE analyses with the observed behaviour of the specimens. The ratio of the predicted shear capacities using the finite element analysis and the experimental shear capacities (V_{exp}/V_{FE}) is 1.03 on average (COV of 0.10) (see Table 2). For specimen S1, with stirrups, the finite element model predicted many diagonal cracks, as shown in Fig. 3, while one critical diagonal crack was predicted for the other specimens. For specimens type P, the finite element predictions agree well with the initiation of two diagonal cracks, the first one leading to failure. Generally, the critical diagonal crack location was predicted to be closer to the midspan loading but both the predicted and experimental critical shear cracks intercept the same number of transverse bars. The predicted strains in the transverse reinforcement (Fig. 6) agree well with the experimental measurements and resulted in good predictions of the behaviour of the specimens. The first shear cracking load is underestimated by 123 kN on average but the overall member behaviour is well predicted. The predicted crack slip δ is smaller than the experimental measurements but the predicted crack widths agree well with the experimental measurements. The predicted strains in Fig. 6 indicate that failure of specimens type T and P occurred without yielding of the transverse reinforcement.

5.3. Shear Resistance Mechanisms

To analyze the shear resistance mechanisms in specimens P1 and P2, V_{exp} versus w is plot in Fig. 10. The shear carried by V_s is determined by the stress in reinforcing bars intercepting the main diagonal crack and derived from Eq.(4) (see Fig. 10). The shear carried by the concrete, V_c, is limited by the aggregate interlock and determined using Eq. (3). The shear carried by the dowel action is determined with Eq. (14) [36, 37], where δ_s is the vertical crack displacement and ℓ_{da} is the length of the splitting crack along the longitudinal reinforcement.

$$V_d = \frac{1.94 d_b^2 A_s E_s}{\ell_{da}^3}\delta_s \le 1.62 A_s \sqrt{f_c' f_y} \quad \text{(MPa, mm units)} \tag{14}$$

The length of the splitting cracks ℓ_{da} determined from the experimental cracking pattern in Fig. 3 is about 700 mm and 760 mm for the members P1 and P2, respectively. By comparing the shear resistance mechanisms in Fig. 10, it can be seen that the shear carried by the dowel action is much lower than other mechanisms. At shear failure, the shear carried by the dowel action is 29.6 kN for the member P1 and 32.5 kN for the member P2, which represents 4.2% and 3.3% of the total shear, respectively. Also, it is found that the summation of the aggregate interlock, the shear reinforcement resistance and the dowel action ($V_c + V_s + V_d$) resulted in lower predictions than the failure shear, V_{exp}. The contribution of a direct compression strut between the loading location and the support (V_{strut}) may also develop and hence play a role in resisting shear [37-46]. This phenomenon is generally more significant for deep members with a ratio a/d lower than 2.5 [38-40] and few models developed in the last decades take into account this mechanism [41-45]. The tested specimens had a shear span to depth ratio of 2.9 and exhibited a few shear cracks, which enabled the development of the direct strut after significant shear cracking. As shown in Fig. 10, at failure of specimens P1 and P2, V_{strut} is about 172 kN and 344 kN, respectively, which represent 24 % and 36% of the total shear. For comparison, the aggregate interlock limits V_c to 138 kN and 100 kN (19% and 10%) and the value of V_s is 377 kN and 494 kN (53% and 51%), respectively for these specimens. Therefore, the concrete strut formation in the uncracked concrete depth contributes to the total shear capacities of both P1 and P2 specimens. Specimens P1 and P2 failed due to concrete crushing in compression, which is associated with the loss of V_{strut}. At a crack width of 3.6 mm at the failure shear of specimen P1, both type P specimens exhibited similar values of V_c, V_s and V_{strut}. At failure specimen P2 had a larger strut component than P1 (see Fig. 10). This is confirmed by the FE results presented in Fig. 11 showing the predicted principal concrete compressive stress, f_{c2}, and shear stress, v_{cxy}, at failure. The orientation of the concrete compressive stress is illustrated by lines in Fig. 11a, which confirm the presence of a compressive stress field between the loading location and the support. Numerical integration of the shear stress in the uncracked concrete depth illustrated in Fig. 11b can be used to estimate V_{strut}. Based on the FE analysis of type P members, one can determine that V_{strut} = 306 kN, which represents 39% of the predicted shear capacity V_{fe}.

6. PARAMETRIC ANALYSIS

A total of 127 finite element analyses were performed to analyze the effects of the shear span-to-depth ratio, vertical pre-stressing, transverse bar spacing and vertical bar stiffness on the shear behaviour of the strengthened member. The properties of the additional concrete members analyzed in this section are presented in Fig. 12 and Table 3. In Table 3, the shear at flexural failure, V_{flex}, was determined according to CSA-S6 [14]. The shear capacity of members without shear reinforcement, V_c was determined from finite element analysis and this value is used in the following section to evaluate the shear strengthening efficiency.

Each additional shear strengthening cases studied utilized unbonded transverse reinforcing bars similar to the ones used for members P1 and P2. To experience a possible size effect in shear, member heights varied between 750 mm and 3000 mm. A mesh similar to the ones used for the experimental tests is used for these members (Fig. 7). Transverse reinforcement ratios, ρ_v, varies between 0 (no shear reinforcement) to $\rho_{v,max}$ (see Table 3), and different end anchorage stiffness values of the shear strengthening were analyzed.

6.1. Shear span to depth ratio

Fig. 13 presents the effect of the shear span-to-depth ratio, a/d, on the ratio between the shear capacity provided by the direct strut action, V_{strut}, and the shear capacity, V_{fe}, both determined by FE analysis. For comparison purposes, two shear reinforcement ratios, ρ_v, are presented as well as the FE capacities determined for the type P and T tested members.

It can be seen that a large part of shear is carried by V_{strut} for $a/d \leq 2.9$ as previously observed for the experiments. However, the contribution of V_{strut} is less ($V_{strut}/V_n < 20\%$) as the shear span-to-depth ratio, a/d, increases. This decreasing of V_{strut} is similar to the one observed by increasing the shear-to-depth ratio of members without shear reinforcement [37, 38].

For members with $a/d > 2.9$, a large number of diagonal cracks were present, yielding of transverse reinforcement crossing the critical diagonal crack was observed and transverse reinforcement between the support and this diagonal crack were highly stressed (up to f_y). For comparison with members $a/d \leq 2.9$ and experimental tests, a large diagonal crack was present, transverse reinforcement crossing the main shear crack did not reach their yielding strength and reinforcement between the support and the crack experienced almost no stress. By increasing the a/d ratio above 2.9, the contribution of V_{strut} significantly decreases while V_s increases.

By comparing same members with different reinforcement ratio, it can be observed that by increasing the shear reinforcement ratio ρ_v the proportion of shear carry by V_{strut} reduces. Generally, members with the same amount of longitudinal reinforcement, shear span-to-depth ratio and material properties exhibit a similar uncracked concrete depth [41-43], which results in a comparable value of V_{strut}. For example, V_{strut} equals 284 kN and 272 kN for the two members P750a illustrated in Fig. 13 (a/d = 2.9, ρ_v =

0.13% and 0.21% respectively). However, a larger amount of transverse reinforcement results in an increased member shear capacity and therefore, in a smaller ratio V_{strut} / V_{fe} as illustrated in Fig. 13.

6.2. Vertical Stiffness

The transverse reinforcement stiffness is defined by the additional equivalent length, ℓ_a, required to represent the total shear reinforcement elongation u_{tot}, which includes the anchorage displacement, according to the bar elongation u_s in Eq. (15). In these finite element analyses, ℓ_a varies between 0 mm (no anchor displacement) and 3500 mm (large part of the vertical displacement is due to the anchorage). It is expected that this range covers a very large range of anchor flexibly. For comparison, specimen P1 experienced u_s = 1.2 and u_{tot} = 4.2 mm, which results in an equivalent length ℓ_a of 1900 mm.

$$\ell_a = \left(\frac{u_{tot}}{u_s} - 1 \right) \ell_{bar} \tag{15}$$

Fig. 14 and Fig. 15 present the shear versus deflection response of member P750b and the maximum shear capacity of members P750a and P750b (see Table 3) for different amounts of transverse reinforcement and shear strengthening system stiffness. While the predictions using CSA-S6 [14] are not applicable for unbonded transverse reinforcement these predictions are shown in Fig. 14 to illustrate the influence of the anchorage flexibility. For the three ρ_v values given in Fig. 14, it can be observed that the initial stiffness of the curves does not significantly differ for the range of the strengthening system stiffness studied. For members with ℓ_a = 0 and ρ_v of 0.13% and 0.17%, a decrease of the shear versus deflection stiffness is initiated at a shear cracking load of about 460 kN. Members with more flexible shear strengthening systems (ℓ_a > 0) experienced an abrupt load decrease which becomes more significant as the amount of transverse reinforcement and the strengthening system stiffness decreases.

However, this sudden load decrease is not observed for members with the highest amount of transverse reinforcement (ρ_v = 0.52%) and $\ell_a \leq$ 1000 mm. These members experienced higher shear cracking loads ranging from 495 kN to 615 kN and their overall stiffness of the load-deflection curves decreases at higher load levels.

It is interesting to observe in Fig. 14 that the decreased stiffness of the strengthening system, with $\ell_a \geq$ 1000 mm, shifts the failure mode of members from ductile bending failures to brittle shear failures with smaller deflections at failure. Generally, the shear capacity decreases as the shear strengthening system stiffness decreases due to a lower shear carried by the unbonded bars. Similar observations were reported by Suntharavadivel [4], Elstner and Hognestad [5].

Fig. 15 illustrates the influence of different shear reinforcement ratios and strengthening stiffness values. For the cases with $\rho_v = 0.07\%$ the transverse reinforcement ratio is less than $\rho_{v,min}$. Members with a very flexible shear strengthening system may experience brittle shear failure instead of a ductile flexural failure. It is clear that a member with very low amount of very flexible shear reinforcement may experience brittle shear failure after shear cracking, consequently no increase of shear strength. This is the case for member P750a with a reinforcing ratio of ρ_v = 0.07% and a very flexible shear strengthening (ℓ_a = 14000 mm not illustrated in Fig. 15).

6.3. Vertical Prestressing

Member P750a was analysed with different amounts of transverse prestressing in the unbounded bars with f_{pv} up to 390 MPa (which includes prestress losses). The effect of vertical prestressing $\rho_v f_{pv}$ (force par unit of concrete area) on shear capacity is illustrated in Fig. 16. It can be seen that vertical prestressing may significantly increases the shear capacity. Since the shear carried by the unbonded bars is a function of the vertical crack displacement, increasing the amount of vertical prestressing reduces the crack width and increases the aggregate interlock. Also, the increase in shear capacity is more significant for members with flexible shear reinforcement (ℓ_a = 2700) than members with stiff shear reinforcement (ℓ_a = 75 mm). For flexible shear strengthening systems, the bar stress at failure is lower than f_y while the addition of prestressing may increase the bar stress up to f_y and V_s consequently increases. For example, the stress in the transverse reinforcement at shear failure increased from 266 MPa to 400 MPa (equals to f_y) with the addition of vertical prestressing of 195 MPa ($\rho_v f_{pv}$ = 0.341 MPa). The same amount of prestressing has no significant effect on the shear capacity for member with ℓ_a = 75 mm since the transverse reinforcement was predicted to reach f_y without prestressing.

7. CONCLUSIONS

This paper examines the shear behaviour of shear critical members with unbonded shear reinforcement placed in holes drilled into the concrete. Eight experimental tests were performed and numerical analyses were carried out. Shear capacities were compared to the predictions using the Canadian Highway Bridge Design Code [14] for shear design and to predictions made with non-linear finite element analyses. The finite element analyses resulted in very accurate predictions of the shear capacities, member responses and cracking patterns. A parametric analysis was carried out to better understand the effect of the shear span-to-depth ratio, amount of unbonded shear reinforcement, the stiffness of the anchorage of the shear strengthening system and the use of vertical prestressing. The following conclusions are made based on this study:

- Unbonded shear reinforcement increases the shear capacity and deformability;

- Propagation of a sudden large diagonal crack caused a drop of the shear for members with unbonded shear reinforcement. This behaviour is very similar to the one observed for members without shear reinforcement at failure.

- After diagonal cracking, a large diagonal crack is required to activate the unbonded shear reinforcement and the concrete shear capacity is limited by aggregate interlock.

- The shear strengthening stiffness significantly affects the shear capacity. Stiff shear reinforcement experienced yielding at shear failure while more flexible unbonded shear reinforcement did not reach yield.

- Vertical prestressing increases the shear strengthening efficiency by increasing the shear capacities. With a sufficient amount of prestressing, members with a flexible shear strengthening system can experience a similar behaviour to members with stiff shear strengthening system;

- The Canadian Highway Bridge Design Code developed from the modified compression field theory implicitly assumes perfect bonded transverse reinforcement and hence is not applicable for prediction the shear capacity of unbonded shear reinforcement.

ACKNOWLEDGEMENTS

The research reported in this paper was made possible by funding from the Natural Sciences and Engineering Research Council of Canada (NSERC, CREATE-INFRA) and the “Fonds de Recherche du Québec – Nature et Technologies” (FRQNT). The authors also acknowledge the contributions of Benoit Cusson and Philippe Provencher who performed the testing in the structures laboratory at Université Laval.

REFERENCES

[1] Mitchell D, Marchand J, Croteau P, Cook WD. Concorde Overpass Collapse: Structural Aspects. Journal of Performance of Constructed Facilities. 2011;25:545-53. https://doi.org/10.1061/(ASCE)CF.1943-5509.0000183

[2] Johnson PM, Couture A, Nicolet R. Commission of Inquiry Into the Collapse of a Portion of the De La Concorde Overpass. Quebec, Canada: Gouvernement du Quebec; 2007. p. 198.

[3] Adhikary BB, Mutsuyoshi H. Shear Strengthening of Reinforced Concrete Beams Using Various Techniques. Construction and Building Materials. 2006;20:366-73. https://doi.org/10.1016/j.conbuildmat.2005.01.024

[4] Suntharavadivel TG. Retrofitting of Shear Damaged Reinforced Concrete Beams. In: Fragomeni S, Venkatesan S, editors. Incorporating Sustainable Practice in Mechanics and Structures of Materials. London UK: Taylor and Francis Group; 2010. p. 197-202.

[5] Elstner RC, Hognestad E. Laboratory Investigation of Rigid Frame Failure. ACI Journals. 1957;28:637-68.

[6] Lechner J, Feix J. Development of an efficient shear strengthening

method for dynamically loaded structures. In: Koichi Maekawa AK, Jun Yamazaki, editor. Proceedings of The 11th fib International PhD Symposium in Civil Engineering. Tokyo, Japan2016. p. 753-61.

[7] Ferreira D, Bairán JM, Marí A. Shear Strengthening of Reinforced Concrete Beams by Means of Vertical Prestressed Reinforcement. Structure and Infrastructure Engineering. 2016;12:394-410. https://doi.org/10.1080/15732479.2015.1019893

[8] Teng S, Kong F-K, Poh SP, Guan LW, Tan K-H. Performance of Strengthened Concrete Deep Beams Predamaged in Shear. ACI Structural Journal. 1996;93:159-71.

[9] El-Shafiey T, Atta A. Retrofitting of Reinforced Concrete Beams in Shear Using External Prestressing Technique. Magazine of Concrete Research. 2012;64:201-2011. https://doi.org/10.1680/macr.10.00157

[10] Inácio MMG, Pinho Ramos A, Faria DMV. Strengthening of Flat Slabs with Transverse Reinforcement by Introduction of Steel Bolts Using Different Anchorage Approaches. Engineering Structures. 2012;44:63-77. http://dx.doi.org/10.1016/j.engstruct.2012.05.043

[11] Altin S, Tankut T, Anil Ö, Demirel Y. Response of Reinforced Concrete Beams with Clamps Applied Externally: An Experimental Study. Engineering Structures. 2003;25:1217-29. https://doi.org/10.1016/S0141-0296(03)00082-8

[12] Khaloo AR. Shear Repair of Reinforced Concrete Beams Using Post-Tensioning. ACI Special Publication. 2000;193:519-49.

[13] Shamsai M, Sezen H, Khaloo A. Behavior of Reinforced Concrete Beams Post-Tensioned in the Critical Shear Region. Engineering Structures. 2007;29:1465-74. https://doi.org/10.1016/j.engstruct.2006.07.026

[14] CSA-S6. Canadian Highway Bridge Design Code and Commentary. 11th ed. Mississauga, ON, Canada: Canadian Standards Association; 2014.

[15] Hilti. Hilti Fastening Technology Manual B 2.11. Schaan, Liechtenstein2005. p. 384.

[16] Collins MP, Mitchell D, Adebar P, Vecchio FJ. A General Shear Design Method. ACI Structural Journal. 1996;93:36-60.

[17] Bentz EC, Collins MP. Development of the 2004 CSA A23.3 Shear Provisions for Reinforced Concrete. Canadian Journal of Civil Engineering. 2006;33:521-34. https://doi.org/10.1139/l06-005

[18] Vecchio FJ, Collins MP. The Modified Compression-Field Theory for Reinforced-Concrete Elements Subjected to Shear. ACI Journal. 1986;83:219-31.

[19] Wong PS, Vecchio FJ, Trommels H. Vector2-User's Manual. 2nd ed. Toronto, Canada: University of Toronto; 2013.

[20] Vecchio FJ. Disturbed Stress Field Model for Reinforced Concrete: Formulation. Journal of Structural Engineering. 2000;126:1070-7. https://doi.org/10.1061/(ASCE)0733-9445(2000)126:9(1070)

[21] Yamamoto T, Vecchio F. Analysis of Reinforced Concrete Shells for Transverse Shear and Torsion. ACI Structural Journal. 2001;98:191-200.

[22] Bentz EC. Sectional Analysis of Reinforced Concrete Members. University of Toronto: University of Toronto; 2000.

[23] Bentz EC. Explaining the Riddle of Tension Stiffening Models for Shear Panel Experiments. Journal of Structural Engineering. 2005;131:1422-5. https://doi.org/10.1061/(ASCE)0733-9445(2005)131:9(1422)

[24] Sato Y, Vecchio FJ. Tension Stiffening and Crack Formation in Reinforced Concrete Members with Fiber-Reinforced Polymer Sheets. Journal of Structural Engineering. 2003;129:717-24. https://doi.org/10.1061/(ASCE)0733-9445(2003)129:6(717)

[25] Vecchio FJ, Lai D. Crack Shear-Slip in Reinforced Concrete Elements. Journal of Advanced Concrete Technology. 2004;2:289-300. https://doi.org/10.3151/jact.2.289

[26] Thorenfeldt E, Tomaszewicz A, Jensen JJ. Mechanical Properties of High-Strength Concrete and Application in Design. In: Ivar Holand NB, editor. Proceedings of the Symposium Utilization of High Strength Concrete. Stavanger, Norway: Tapir; 1987. p. 149-59.

[27] Collins MP, Mitchell D. Prestressed Concrete Structures. Englewood Cliffs, New Jersey, USA: Prcnticc-Hall; 1991.

[28] Ottosen NS. Constitutive Model for Short-Time Loading of Concrete. Journal of the Engineering Mechanics Division ASCE. 1979;105:127-41.

[29] Vecchio FJ. Finite Element Modeling of Concrete Expansion and Confinement. Journal of Structural Engineering. 1992;118:2390-406. https://doi.org/10.1061/(ASCE)0733-9445(1992)118:9(2390)

[30] Collins DM, Klingner RE, Polyzois D. Load Deflection Behavior of Cast-in-place and retrofit concrete anchors subjected to static fatigue and impact tensile loads. Austin, Texas 78712-1075: Center for Transportation Research, The University of Texas at Austin; 1989. p. 241.

[31] Hilti. HSL-3 / HSL-GR Submission Folder. Austria: Hilti Corporation; 2013.

[32] Balazs GL. Cracking Analysis Based on Slip and Bond Stresses. ACI Materials Journal. 1993;90:340-8.

[33] Lee S-C, Cho J-Y, Vecchio FJ. Model for Post-Yield Tension Stiffening and Rebar Rupture in Concrete Members. Engineering Structures. 2011;33:1723-33. https://doi.org/10.1016/j.engstruct.2011.02.009

[34] fib. fib Model Code for Concrete Structures 2010. Lausanne, Switzerland: Ernst and Sohn; 2013.

[35] Debernardi PG, Taliano M. An Improvement to Eurocode 2 and fib Model Code 2010 Methods for Calculating Crack Width in RC Structures. Structural Concrete. 2016;17:365-76. https://doi.org/10.1002/suco.201500033

[36] He XG, Kwan AKH. Modeling Dowel Action of Reinforcement Bars for Finite Element Analysis of Concrete Structures. Computers and Structures. 2001;79:595-604.

[37] Francesco C, Miguel FR, Aurelio M. An analysis of the shear-transfer actions in reinforced concrete members without transverse reinforcement based on refined experimental measurements. Structural Concrete. 2018;19:49-64. doi:10.1002/suco.201700145

[38] Kani MW, Huggins MW, Kani G, Wittkopp RR. Kani on Shear in Reinforced Concrete. Toronto, ON, Canada: University of Toronto, Dept. of Civil Engineering; 1979.

[39] Collins MP, Bentz EC, Sherwood EG. Where is Shear Reinforcement Required? Review of Research Results and Design Procedures. ACI Structural Journal. 2008;105:590-600.

[40] Muttoni A, Fernández Ruiz M. Shear Strength of Members Without Transverse Reinforcement as Function of Critical Shear Crack Width. ACI Structural Journal. 2008;105:163-72.

[41] Cladera A, Marí A, Ribas C, Bairán J, Oller E. Predicting the shear–flexural strength of slender reinforced concrete T and I shaped beams. Engineering Structures. 2015;101:386-98. https://doi.org/10.1016/j.engstruct.2015.07.025

[42] Cladera A, Marí A, Bairán J-M, Oller E, Ribas C. One-Way Shear Design Method Based on a Multi-Action Model: A compromise between simplicity and accuracy. Concrete International. 2017;39:40-6.

[43] Frosch RJ, Qiang Y, Cusatis G, Bažant ZP. A Unified Approach to Shear Design. Concrete International. 2017;39:47-52.

[44] Hong-Gun P, Kyoung-Kyu C. Unified Shear Design Method of Concrete Beams Based on Compression Zone Failure Mechanism. Concrete International. 2017;39:59-63.

[45] Tureyen AK, Frosch RJ. Concrete Shear Strength: Another Perspective. ACI Structural Journal. 2003;100. 10.14359/12802

[46] Kani GNJ. The Riddle of Shear Failure and its Solution. ACI Journal. 1964;61:441-68. 10.14359/7791

FIGURE CAPTIONS

Fig. 1: Shear strengthening systems used for specimen types a) T with expansion anchors and bolted plates, and b) P with bolted plates

Fig. 2: Tested strengthened members (dimensions in mm)

Fig. 3: Comparison between experimental and predicted cracking pattern at failure

Fig. 4: Response of tested specimens with transverse reinforcement and FE predictions of the shear, crack width, w, and crack slip, δ, versus the member deflection

Fig. 5: Experimental and FE predictions of shear load and crack width versus member deflection for specimens without transverse reinforcement

Fig. 6: Experimental shear versus transverse reinforcement strain and FE predictions

Fig. 7: Mesh of the specimen T1 and boundary conditions

Fig. 8: Modelling approach for specimen types a) S with stirrups, b) P with bolted plates and c) T with expansion anchors and bolted plates

Fig. 9: Behaviour of concrete a) in tension and b) in compression, c) steel and d) expansion anchorages

Fig. 10: Shear resistance mechanisms vs crack width for specimens P1 and P2

Fig. 11: FE predictions of a) compressive and b) shear stresses at failure for type P members (MPa, mm)

Fig. 12: FE parametric analysis tested members

Fig. 13: Ratio between the shear carried by a direct strut action V_{strut} and the member capacity V_{fe}, both determined by FE analysis, according to the shear span-to-depth ratio.

Fig. 14: Shear versus deflection response of member P750b with different anchor stiffness and transverse reinforcement ratios of 0.13%, 0.17% and 0.52% (ℓ_a in mm)

Fig. 15: Effect of transverse stiffness on shear capacities (black and grey symbols indicate shear and flexural failure respectively)

Fig. 16: Effect of vertical prestressing on shear capacities and shear cracking load for member P750a

Fig. 1

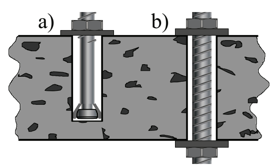

Fig. 2

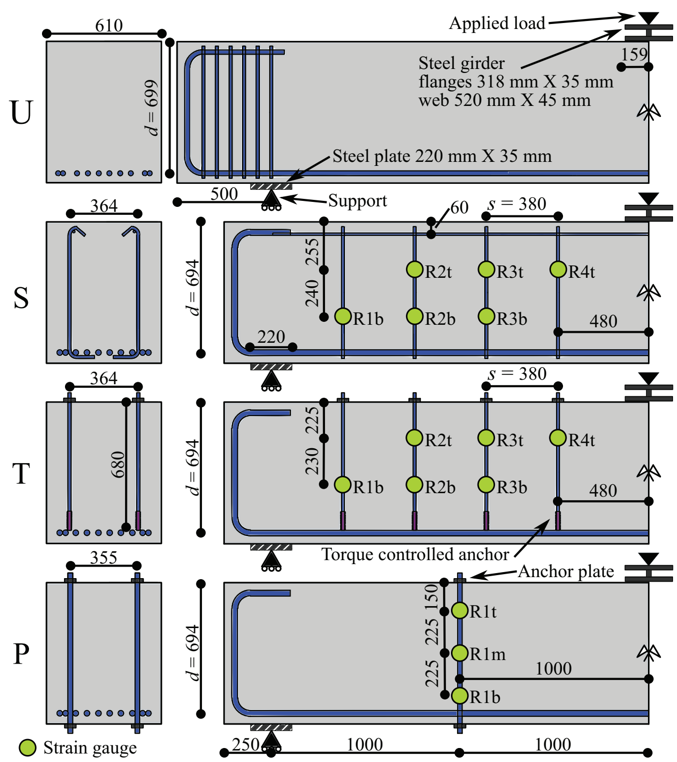

610
d = 699
U
Applied load
Steel girder
flanges 318 mm X 35 mm
web 520 mm X 45 mm
159
Steel plate 220 mm X 35 mm
500
Support
364
S
d = 694
255
240
60
s = 380
R2t
R3t
R4t
R1b
R2b
R3b
480
220
364
T
680
d = 694
225
230
s = 380
R2t
R3t
R4t
R1b
R2b
R3b
480
Torque controlled anchor
Anchor plate
355
P
d = 694
150
225
225
R1t
R1m
R1b
1000
Strain gauge
250
1000
1000

Fig. 3

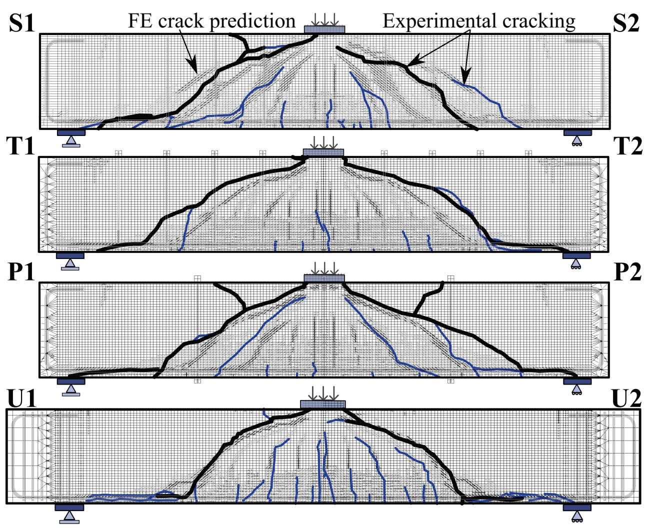

S1
FE crack prediction
Experimental cracking
S2
T1
T2
P1
P2
U1
U2

Fig. 4

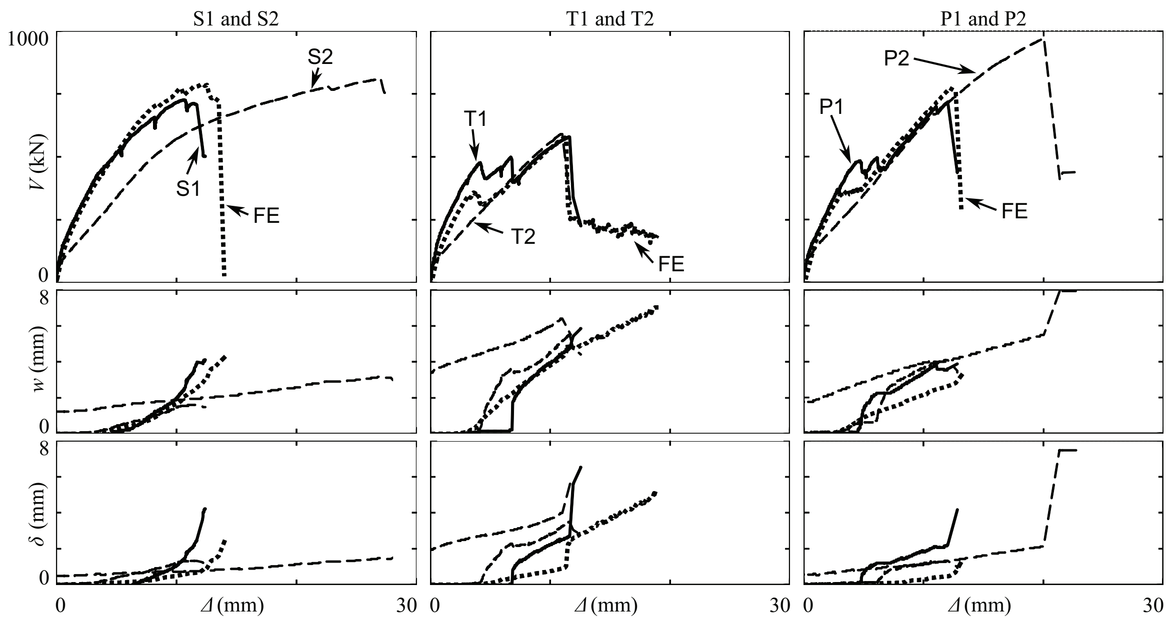

S1 and S2
T1 and T2
P1 and P2
1000
0
V (kN)
S2
S1
FE
T1
T2
FE
P2
P1
FE
8
0
w (mm)
8
0
δ (mm)
0
Δ (mm)
30
0
Δ (mm)
30
0
Δ (mm)
30

Fig. 5

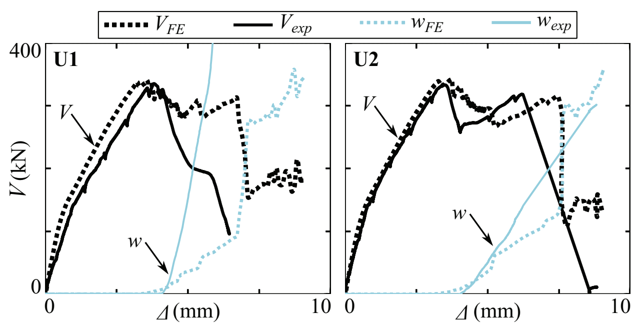

Fig. 6

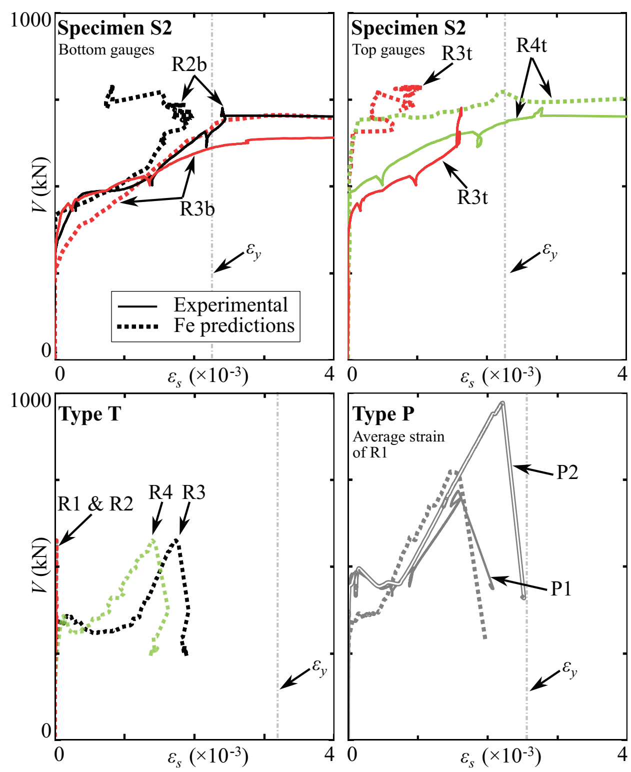

Specimen S2
Bottom gauges
R2b
R3b
Experimental
Fe predictions
1000
0
V (kN)
ε_y
0
ε_s (×10⁻³)
4
Specimen S2
Top gauges
R3t
R4t
R3t
ε_y
0
ε_s (×10⁻³)
4
Type T
R1 & R2
R4
R3
1000
0
V (kN)
ε_y
0
ε_s (×10⁻³)
4
Type P
Average strain
of R1
P2
P1
ε_y
0
ε_s (×10⁻³)
4

Fig. 7

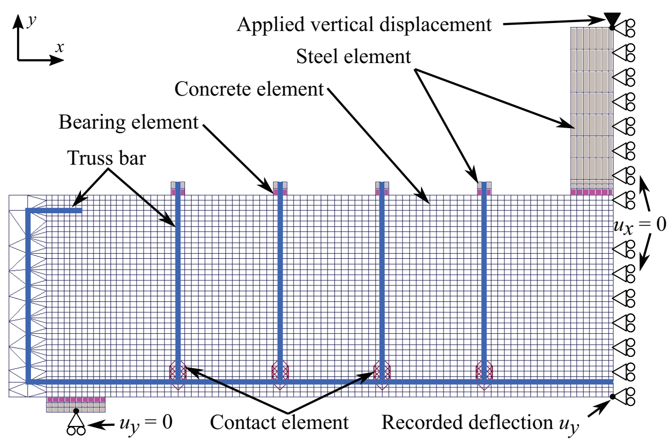

y
x
Applied vertical displacement
Steel element
Concrete element
Bearing element
Truss bar
$u_x = 0$
$u_y = 0$
Contact element
Recorded deflection u_y

Fig. 8

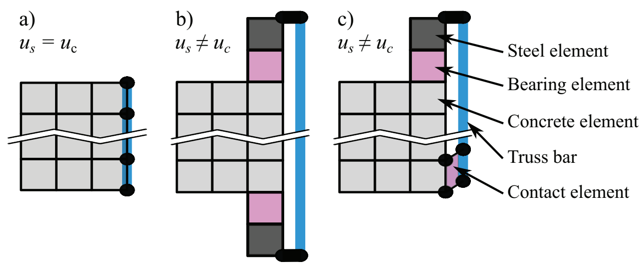

a)
$u_s = u_c$
b)
$u_s \neq u_c$
c)
$u_s \neq u_c$
Steel element
Bearing element
Concrete element
Truss bar
Contact element

Fig. 9

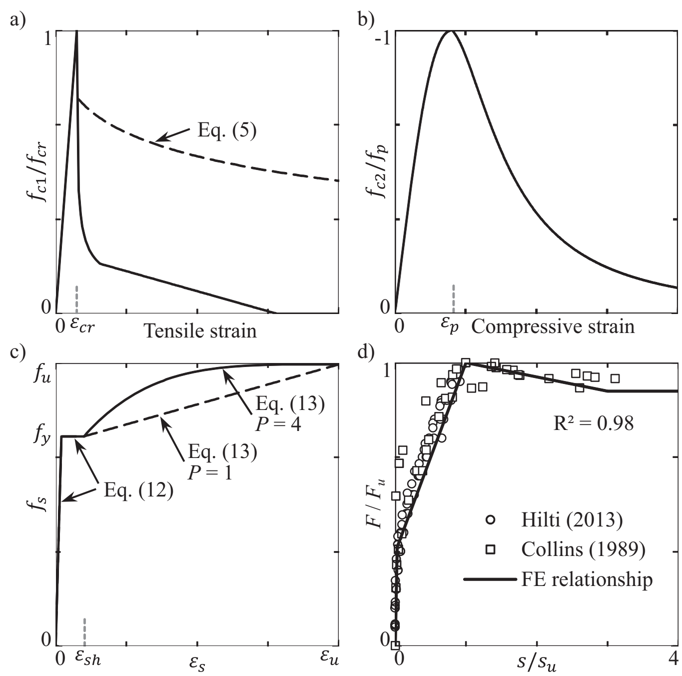

a)
1
0
0
ε_{cr}
Tensile strain
f_{c1}/f_{cr}
Eq. (5)
b)
-1
0
0
ε_p
Compressive strain
f_{c2}/f_p
c)
f_u
f_y
f_s
0
0
ε_{sh}
ε_s
ε_u
Eq. (13) $P = 4$
Eq. (13) $P = 1$
Eq. (12)
d)
1
0
0
4
s/s_u
F / F_u
R² = 0.98
Hilti (2013)
Collins (1989)
FE relationship

Fig. 10

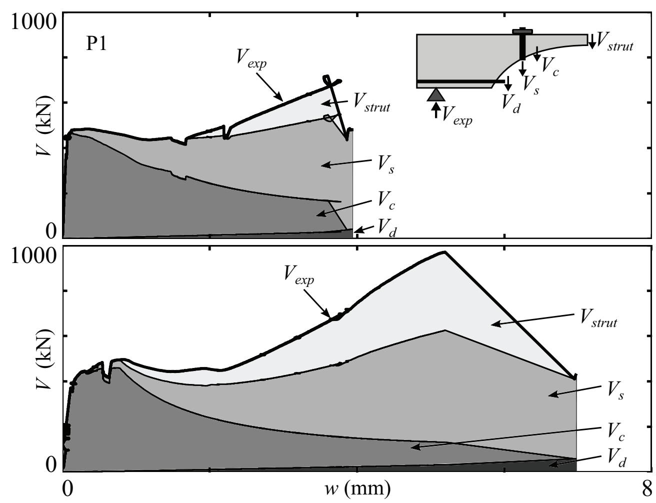

P1
1000
0
V (kN)
V_{exp}
V_{strut}
V_s
V_c
V_d
1000
0
V (kN)
V_{exp}
V_{strut}
V_s
V_c
V_d
0
w (mm)
8

Fig. 11

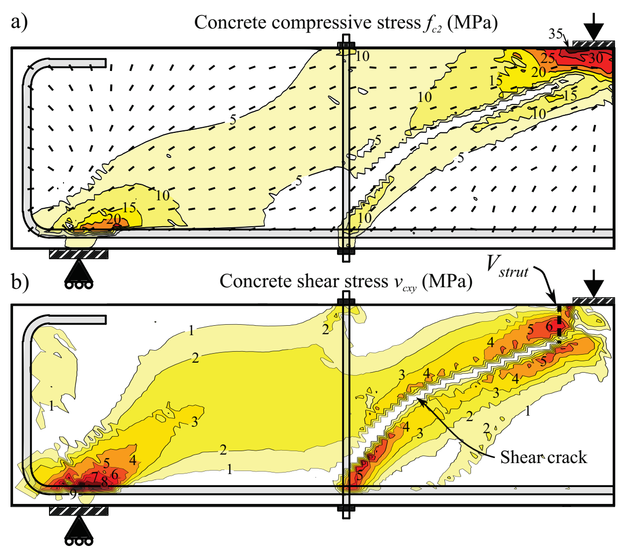
a)
Concrete compressive stress f_{c2} (MPa)
35
30
25
20
15
10
5
b)
Concrete shear stress v_{cxy} (MPa)
V_{strut}
Shear crack
1
2
3
4
5
6
7
8

Fig. 12

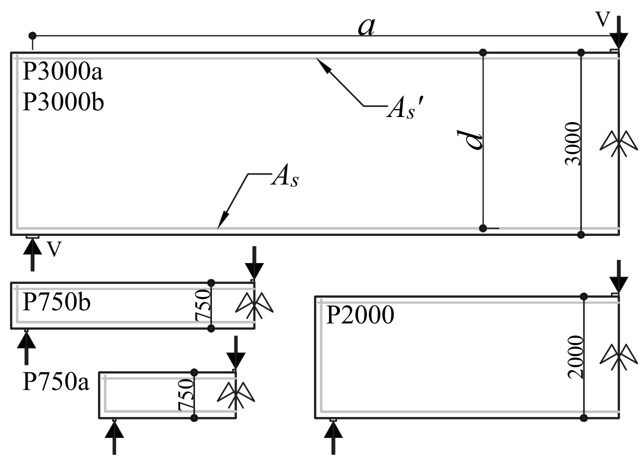

Fig. 13

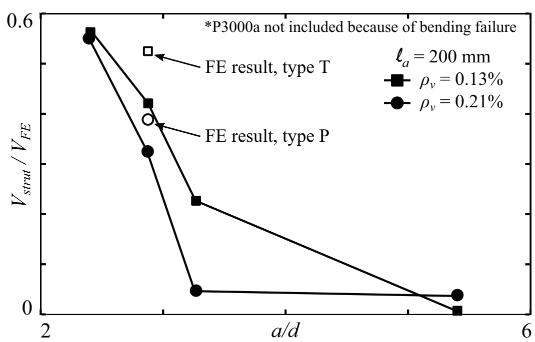
*P3000a not included because of bending failure
ℓ_a = 200 mm
ρ_v = 0.13%
ρ_v = 0.21%
FE result, type T
FE result, type P
0.6
0
2
6
a/d
V_{strut} / V_{FE}

Fig. 14

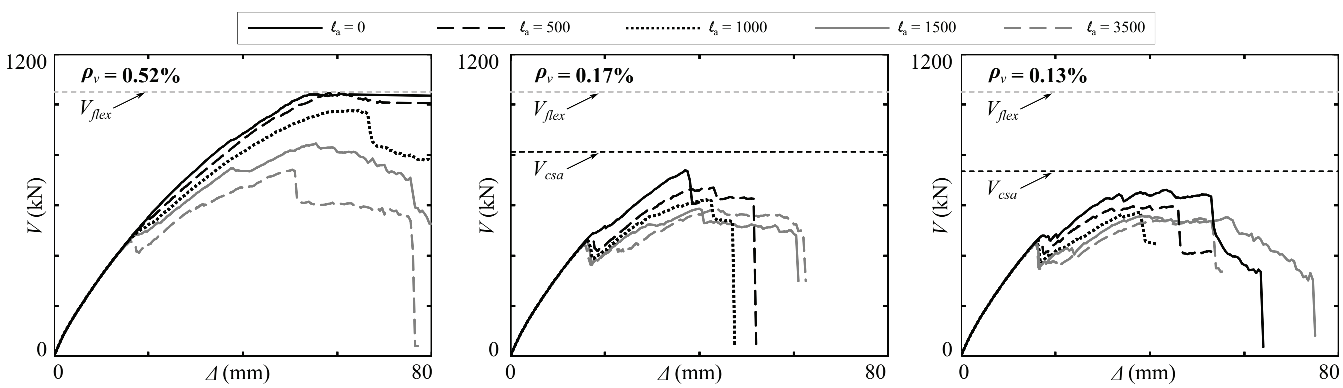

ℓa = 0
ℓa = 500
ℓa = 1000
ℓa = 1500
ℓa = 3500
ρv = 0.52%
ρv = 0.17%
ρv = 0.13%
Vflex
Vcsa
V (kN)
Δ (mm)
1200
0
80

Fig. 15

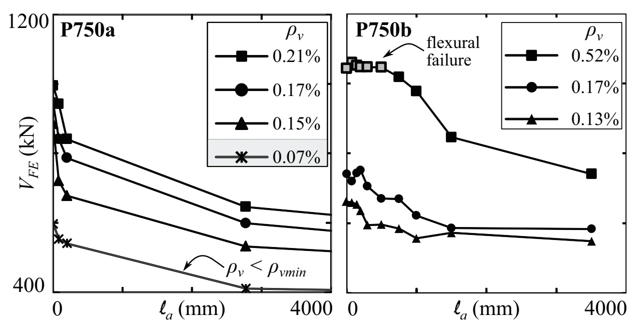

P750a
ρ_v
0.21%
0.17%
0.15%
0.07%
$\rho_v < \rho_{vmin}$
1200
400
V_{FE} (kN)
0
ℓ_a (mm)
4000
P750b
flexural
failure
ρ_v
0.52%
0.17%
0.13%
0
ℓ_a (mm)
4000

Fig. 16

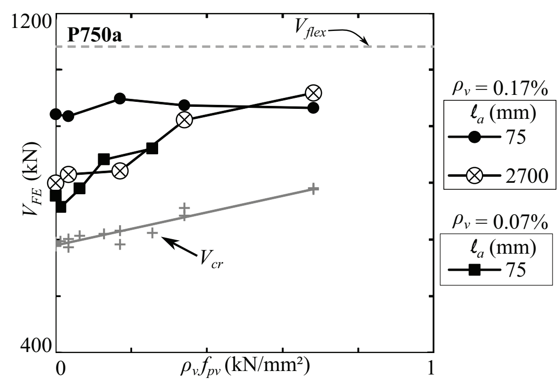

P750a
V_{flex}
V_{cr}
1200
400
V_{FE} (kN)
0
1
$\rho_v f_{pv}$ (kN/mm²)
ρ_v = 0.17%
ℓ_a (mm)
75
2700
ρ_v = 0.07%
ℓ_a (mm)
75

Table 1: Concrete and shear reinforcement properties

Type	Strengthening system	f_c' MPa	E_c MPa	A_v mm²	s mm	f_y MPa	f_u MPa
U	None	34.5	29406	-	-	-	-
S	Stirrups	33.3	25705	400	380	447	633
T	Expansion	31.5	24144	292	380	642	800
P	Plate	31.2	25333	1290	1000	517	690

Table 2: Experimental results at shear cracking and at shear failure, and comparison to predictions

	Critical shear cracking				Maximum shear capacity						
	Test		FE		Test			CSA		FE	
Test	V_{cr}	Δ_{cr}	$V_{cr,FE}$	$\frac{V_{cr,FE}}{V_{cr}}$	V_{exp}	Δ_{exp}	w_{max}	V_n	$\frac{V_n}{V_{exp}}$	V_{FE}	$\frac{V_{FE}}{V_{exp}}$
	kN	mm	kN		kN	mm	mm	kN		kN	
U1	337	7.6	368	1.09	343	7.6	<0.1	389	1.13	378	1.10
U2	341	7.7	368	1.08	341	7.7	<0.1	379	1.11	378	1.11
S1	495	4.7	384	0.78	726	10.7	2.5	804	1.11	786	1.08
S2	484	4.5	384	0.79	809	27.1	3.2	804	0.99	786	0.97
T1	499	6.7	367	0.74	579	11.6	4.7	810	1.40	596	1.03
T2	476	4.2	367	0.77	590	11.0	6.4	810	1.37	596	1.01
P1	484	4.7	365	0.76	717	12.0	3.6	920	1.28	789	1.10
P2	497	6.1	365	0.74	969	20.1	5.5	920	0.95	789	0.81
Avg				0.84					1.17		1.03
COV				0.18					0.14		0.10

Table 3: Members properties for the parametric analysis

Beam	h	d	a/d	ρ	A'_s	$\rho_{v\ max}$	V_{flex}	V_c	n
	mm	mm	mm	%	mm²	%	kN	kN	
P750a	750	694	2.9	1.65	400	0.33	1081	387	52
P750b	750	694	5.4	3.31	400	0.52	913	436	42
P2000	2000	1944	2.4	0.59	800	0.13	1397	524	6
P3000a	3000	2944	3.3	0.39	7000	0.26	1051	774	6
P3000b	3000	2944	3.3	1.02	7000	0.26	2686	1028	21
Total									127

For all beams, b_w = 610 mm, a_g = 20 mm, f'_c = 34.5 MPa

For longitudinal reinforcement, E_s = 200 000 MPa, f_y = 508 MPa

For shear reinforcement, ρ_v between 0 and $\rho_{v,max}$, f_y = 448 MPa